J. Earth Syst. Sci. (2020)129 80
https://doi.org/10.1007/s12040-020-1352-x

© Indian Academy of Sciences

Assessment of spatio-temporal distribution of CO_2 over greater Asia using the WRF–CO_2 model

Srabanti Ballav[1], Manish Naja[1,*], Prabir K Patra[2], Toshinobu Machida[3] and Hitoshi Mukai[3]

[1]*Aryabhatta Research Institute of Observational Sciences (ARIES), Manora Peak, Nainital 263 001, India.*
[2]*RIGC-ESS/IACE, Japan Agency for Marine-Earth Science and Technology (JAMSTEC), Yokohama 2360001, Japan.*
[3]*Center for Global Environmental Research, National Institute for Environmental Studies (NIES), Onogawa, Tsukuba, Ibaraki 3050053, Japan.*
**Corresponding author. e-mail: manish@aries.res.in*

MS received 28 June 2019; revised 26 October 2019; accepted 14 December 2019

In-depth knowledge of global and regional carbon budget is required for effective policymaking to mitigate the global climate change. However, Asian carbon budget shows large uncertainty due to both lack of sufficient observations and detailed understanding of the existing CO_2 observations. A regional air quality model (WRF–CO_2) is set up for simulating atmospheric CO_2 variations over the greater Asia region (68–124°E, 2°S–45°N) for the period 2010–2012. The WRF–CO_2 simulations are compared with observations from nine sites and a global Atmospheric Chemistry Transport Model (ACTM). The comparisons suggest WRF–CO_2 simulation is able to capture large scale features in the observed variabilities, with varied ability at fine scales depending on representation of surface fluxes and meteorology around the observation sites. Analysis of CO_2 signals from individual flux components suggests that ocean flux has least contribution to the CO_2 variation (<10%). Four sites (Mt. Waliguan, Nainital, Cape Rama and Lulin) show dominance of biospheric flux over fossil flux to the CO_2 variation (>80%). CO_2 mixing ratios are found to be maximum in northern hemisphere (NH) winter over East Asia, while they are maximum in NH spring over Indian subcontinent. Observed peak-to-trough seasonal amplitude is lowest (4.5 ppm) for the site Bukit Koto Tabang, Indonesia and highest (29.5 ppm) for Shangdianzi in China. Statistical analysis from monthly mean CO_2 time series shows that correlation coefficient and normalised standard deviation with observations, are generally equal or better for the WRF–CO_2 than the coarser resolution ACTM. Study of synoptic scale CO_2 variations shows that the WRF–CO_2 is able to better resolve daytime signatures than those in the night. Year-to-year CO_2 variations of seasonal cycle amplitude is highest ($\sim$5 ppm) at Nainital, India compared to all other sites.

Keywords. CO_2 simulation; WRF–CO_2; Asia; CO_2 seasonal cycle.

1. Introduction

Global mean carbon dioxide (CO_2) concentration has increased to more than 400 ppm from $\sim$277 ppm in the preindustrial era (1750) (Joos and Spahni 2008; Dlugokencky *et al.* 2017). CO_2 is the most important anthropogenic species with largest contribution (55.5%) to warming effect on the earth's atmosphere during the period 1750–2010, leading to adverse impacts on climate

Published online: 26 February 2020

(IPCC 2014). The recent CO_2 growth rate of about 2 ppm/yr is attributed to fast economic growth in the Asian countries (e.g., Le Quéré *et al.* 2018). India is the third largest CO_2 emitter with ∼2.5 $GtCO_2$/yr in 2017, after China (∼9.8 $GtCO_2$/yr) and USA (∼5.3 $GtCO_2$/yr), and has the fastest increase rate in the world since 2013 (Le Quéré *et al.* 2018). In the case of India, though the per capita CO_2 emission is much lower (1.8 tCO_2/person) compared to other developed countries (e.g., USA 16.2 tCO_2/person) in 2017, emission rate has been fastest (3.9%) from the year 2016 to 2017 (Le Quéré *et al.* 2018). Prominent contributions from the emerging economies have been intended for mitigation of greenhouse gases emission increase under the Paris Agreement for keeping the global average temperatures rise below 2°C as discussed during the 2015 UNFCCC (United Nations Framework Convention on Climate Change) Conference of the Parties (COP-21).

Quantification of regional carbon budget by inverse or top down approach shows large uncertainty (∼150%) over South Asia (Patra *et al.* 2013) for net biospheric flux of CO_2 compared to other developed countries, such as Europe (∼30%; Luyssaert *et al.* 2012) and USA (∼60%; King *et al.* 2015). This is mainly due to uncertainty in the forward transport model, sparse observational networks and lack of high temporal variation data (Sundareshwar *et al.* 2007). The high-resolution forward transport model simulations of CO_2 at hourly to synoptic timescales could bridge the data gap in this least studied region (Sarrat *et al.* 2007; Pillai *et al.* 2009; Ballav *et al.* 2012; Kou *et al.* 2015).

Asia has versatile land use, terrestrial ecosystem and unique climate dynamics. This could be seen by the role of South Asian summer monsoon circulation (June–September) and western disturbance (December–March) influencing the biospheric fluxes due to change in vegetative growths and crop cultivations. Moreover, owing to strong convection during monsoon season, long lived (GHGs) and short-lived trace gases from South Asia are vertically lifted up and redistributed to other region of the world (Bhattacharya *et al.* 2009; Lin *et al.* 2015; Chandra *et al.* 2017). It has also been shown that synoptic and mesoscale events which have seasonal reversal are not satisfactorily represented by the global model over the continent and coastal regions (Patra *et al.* 2008, 2009; Barnston *et al.* 2010). Observations from Himalayan region are also not well represented by the global models due to their coarse spatial resolution. On the contrary, the meteorology over South Asia is well simulated by the Weather Research Forecast-Chemistry (WRF–Chem) model (Kumar *et al.* 2012; Naja *et al.* 2016).

Modelling studies for verifying the quality of the known source and sink of CO_2 have not yet been carried out over greater part of the Asian landscapes. Moreover, very few model studies were conducted over large parts of Asian region for CO_2 transport (e.g., Patra *et al.* 2008; Tiwari *et al.* 2011). Previous efforts by Ballav *et al.* (2012, 2016) highlighted the advantage of using a high-resolution online regional model for CO_2 transport instead of a coarser resolution global model over the East Asia region. Recent expansion of the *in-situ* measurement sites in Asia, providing continuous or discrete CO_2 data, provides a unique opportunity to better understand the regional CO_2 variations.

Here, we analyse the spatio-temporal distribution of CO_2 by using an online and high-resolution regional model for CO_2 (WRF–CO_2; Ballav *et al.* 2012) for the first time covering a wide range of sites over the greater Asia region for three years (2010–2012). Performances of the WRF–CO_2 model simulations are compared with the observed atmospheric CO_2 mixing ratios at nine sites in different environmental conditions over South/East/Southeast Asia. The sites cover remote mountain, tropical rainforest, urban, deserts, grassland, and coastal environments. In addition, the WRF–CO_2 simulation results are also compared with results from a global model JAMSTEC's ACTM (Patra *et al.* 2009). A description of the models, input/observation data is given in section 2, followed by results in section 3. Summary and conclusions are presented in section 4.

2. Methodology

2.1 *Observation sites and WRF–CO_2 model set-up*

Carbon dioxide data from nine ground-based sites are used here to compare with model simulations. Data from eight stations are obtained from the World Data Centre for Greenhouse Gases (WDCGG 2016) and data from Nainital (NTL), India are collected jointly by the ARIES, India and NIES, Japan. A brief description of nine observation stations is provided in table 1, and locations are depicted in figure 1.

Table 1. *Details of CO_2 observational sites used in the present study. Model height of the observation site is also provided.*

Stations, lat., long., height (amsl)	Country	Model height of site (m)	Description	Data interval and period
Bukit Koto Tabang (BKT), 0.20°S, 100.32°E, 864 m	Indonesia	712.3	Remote continental hill	Hourly data (2010–2012)
Danum Valley (DMV), 4.97°N, 117.83°E, 426 m	Malaysia	330.3	Mountain valley	Hourly data (2010)
Cape Rama (CRI), 15.08°N, 73.83°E, 60 m	India	34.0	Coastal	Event data (15 days) (2010–2012)
Hok Tsui (HKG), 22.21°N, 114.26°E, 60 m	Hong Kong (China)	61.3	Remote coastal	Daily data (2010–2012)
King Park (HKO), 22.31°N, 114.17°E, 65 m	Hong Kong (China)	61.3	Small hilly terrain	Daily data (2010–2012)
Lulin (LLN), 23.47°N, 120.87°E, 2867 m	China	1895.6	Inland mountain	Event data (7 days) (2010–2012)
Nainital (NTL), 29.36°N, 79.45°E, 1958 m	India	813.6	Inland mountain	Event data (7 days) (2010–2012)
Mt. Waliguan (WLG), 36.28°N, 100.90°E, 3810 m	China	3143.8	Plateau desert	Daily data (2010–2012)
Shangdianzi (SDZ), 40.65°N, 117.12°E, 287 m	China	474.7	150 km away from Beijing	Event data (15 days) (2010–2012)

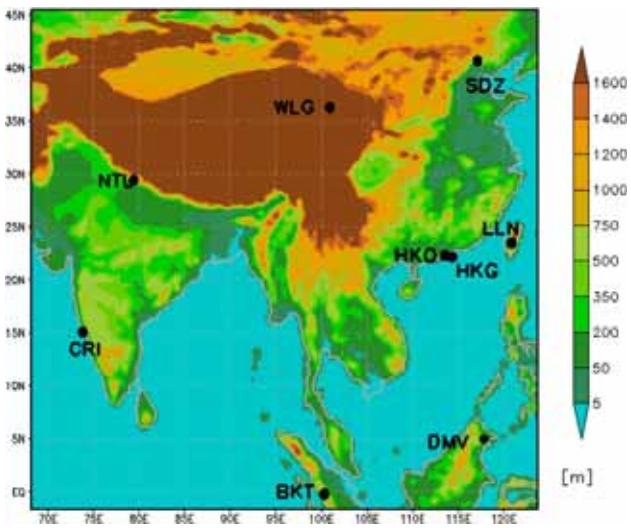

Figure 1. Model domain with terrain height in meter (colour bar). Nine observation sites are also shown. Please refer table 1 for complete name of the sites. Hok Tsui (HKG) and King Park (HKO) are overlapping due to the proximity. Dark brown colour implies model terrain height is above 1600 m.

A coupled online state-of-the-art, regional air quality model Weather Research Forecast coupled with Chemistry (WRF–Chem; Grell *et al.* 2005) is used for CO_2 simulation (WRF–CO_2; Ballav *et al.* 2012). WRF–Chem is a mass and scalar conserving air quality model dealing with chemically reactive aerosol and gases. Since, the original version of WRF–Chem does not include CO_2 species, the model has been modified to incorporate anthropogenic, biogenic and oceanic CO_2 fluxes as non-reactive tracers, and thus referred to as WRF–CO_2. For the present simulation, WRF–CO_2 was configured with horizontal resolution of 27 × 27 km and vertical resolution of 30η layers. The height range is covered from surface up to 100 hPa, with 11 layers located within 2 km from the surface. The model horizontal domain (figure 1) is made to cover most part of the populous Asia and defined on Mercator projection centered at 24°N and 96°E (Myanmar) having 200 × 190 grid points in latitude and longitude. The model domain extended from 68° to 124°E in longitude, and 2°S to 45.2°N in latitude. WRF–Chem has multiple physical, dynamical and chemical options suitable for a broad spectrum of applications. Table 2 summarizes the WRF–CO_2 configuration options of different atmospheric processes that are selected for the present set-up, adopted from Takigawa *et al.* (2007) and Niwano *et al.* (2007). Here, we have provided a brief description of the model and more details could be seen in Ballav *et al.* (2012).

Three dimensional grid analysis nudging is performed to WRF model simulated meteorological fields that initialized using the National Centers for Environmental Prediction (NCEP) final analysis (FNL) data of horizontal winds (U, V) and temperature (T) for the reproduction of realistic tracer transport. Model simulations are sampled horizontally at the nearest grid point of observation sites, and vertically at the lowest model level

Table 2. *Overview of WRF–CO_2 model configuration used in this work.*

Processes	WRF–CO_2 options
Input flux	
Biospheric model data	CASA – 3 hourly
Fossil flux	Edgar 4.2
Ocean flux	Takahashi *et al.* (2009)
Simulation set-up	
Model Centre	24°N and 96°E
Model resolution	27 × 27 km
Model grid	200 (North–South) and 190 (East–West)
Map projection	Mercator
Initial and boundary condition	
Meteorology	NCEP FNL GRIB-2 data
Tracer CO_2	ACTM model
Surface characteristics	
Topography, land use, etc.	10 m USGS data
Physics scheme	
Microphysics	Cowry Single-Moment 3-Class scheme
Longwave radiation	RRTM scheme
Shortwave radiation	Goddard shortwave
Surface layer	Eta similarity
Land surface	Noah Land Surface Model
Planetary boundary layer	MYJ scheme
Cumulus parameterisation	Grell–Devenyi ensemble scheme
Chemistry scheme	
Photolysis, dry deposition, gas phase chemistry, aerosol chemistry, wet scavenging, cloud chemistry	Off
Dynamic scheme	
Vertical turbulent mixing and subgrid convective transport	On
Integration procedure	
Time integration	The 2nd and 3rd order Runge–Kutta Scheme along with a small split time step for acoustic and gravity wave modes
Spatial integration	5th order evaluation of the horizontal flux advection and the 3rd order evaluation of the vertical flux divergence

or the vertical level data is interpolated to the level of observation point (later referred as actual level). The model output is stored in 1-hr interval and is sampled at the nearest observational time of respective sites. Different components of CO_2 like fossil fuel CO_2, terrestrial biosphere CO_2 and ocean CO_2, corresponding to three prescribed fluxes (section 2.2), are treated in the model as non-reactive tracers whose mixing ratios are calculated from atmospheric transport involving advection, cumulus convection and turbulent diffusion.

2.2 *Anthropogenic emissions and the natural fluxes*

Anthropogenic emissions due to fossil fuel consumption and cement production are adopted from the yearly global map of Emission Database for Global Atmospheric Research (EDGARv4.2 2011) with grid resolution of 0.1° × 0.1° (referred as FT). The EDGARv4.2 anthropogenic data are available until 2010 and linearly extrapolated within the domain for rest of the years (2011–2012) without accounting for variation of the regional trends. Terrestrial biospheric surface fluxes are taken from the Carnegie-Ames-Stanford-Approach (CASA) global model having 1° × 1° spatial resolution and 3 hourly temporal resolutions (Olsen and Randerson 2004). The oceanic exchange at 4° × 5° resolution is given as monthly mean air—sea exchange rate of CO_2 from the Lamont–Doherty Earth Observatory (LDEO) (Takahashi *et al.* 2009). Though the fossil flux has very high spatial resolution, due to coarser resolution of biospheric and oceanic flux and limitation of computational facility, we have not increased the

model resolution much than the present one. Although some of the land biosphere models are run at higher spatial resolution than 1° × 1°, well-tested sub-daily time interval data are not available due to the inadequacy of surface forcing data required for land models (Sitch *et al.* 2008; Le Quéré *et al.* 2018). Fluxes are interpolated into model grids using five points running mean and then fitted data is used to get fluxes at model grid adopting the method given by Krishnamurti *et al.* (1998).

2.3 *Initial and boundary conditions*

Initial/boundary conditions (IC/BC) for meteorology are adopted from NCEP final analysis (FNL) GRIB-2 data having temporal resolution 6 hrs and spatial resolution 1° × 1°. Initial condition and boundary condition for atmospheric CO_2 are taken from JAMSTEC's ACTM providing 2.8° × 2.8° resolution field at three hourly intervals (Patra *et al.* 2009). The United States Geological Survey (USGS) data at 10 min resolution is used for the static geographical fields such as land-use and land cover, terrain height and soil type, etc. Three years continuous simulation has been performed from 1st January 2010 to 31st December 2012. First five days model simulation are cut-off as spin up period from the analysis of the model results. In both models, data are used from lowest level of the model, unless it is mentioned (for the WRF–CO_2).

2.4 *Time series data analysis to study variabilities*

Each time series of observed and simulated CO_2 are decomposed into synoptic, seasonal and inter-annual variabilities using a digital filtering technique (Nakazawa *et al.* 1997). The filtering is applied to three years (2010–2012) time period of daily averaged CO_2 data. Three Fourier harmonics are used for representing the smooth seasonal cycle, in addition, two low-pass recursive digital filters are used of the order of 16 and 26 to obtain short-term variation in seasonal cycle and long-term variation in trend, respectively. One to 10-day variations are considered as synoptic scale variation of CO_2. Therefore, synoptic scale variation of CO_2 is obtained by subtracting the smooth fitted curve from daily average data.

3. Results and discussions

3.1 *Spatio-temporal variations*

The WRF–CO_2 simulated CO_2 mixing ratios for four different seasons are depicted in figure 2(a–d). Because the three flux tracers are run as non-reactive, their linearity with fluxes allow to construct model CO_2 concentrations by adding the three separate components (sometimes referred to as Total CO_2). The running of three separate tracers helps us to analyse their contributions to the CO_2 variabilities. The biospheric CO_2 (figure 2e–h), fossil CO_2 (figure 2i–l) and ocean CO_2 (figure 2m–p) components are also shown. CO_2 mixing ratios are maximum in winter over the eastern China. However, CO_2 values are maximum in spring over the Indian subcontinent, including part of Southeast Asian region and western China. Additionally, spring maximum CO_2 values over these regions are much lower than those over the eastern China. Winter time lower CO_2 values over northern India may be attributed to active uptake by the crops and forest ecosystems under the influence of the western disturbances, and lower heterotrophic respiration moderate surface air temperature (Patra *et al.* 2011; Umezawa *et al.* 2016). It is noted that fossil fuel contributes to the maximum increase of CO_2 in winter (figure 2i–l) over the eastern China region. This is corroborated with the energy consumption coupled with the lower boundary layer height over the east Asia leading to enhancement of CO_2 in winter (e.g., Ballav *et al.* 2016; for Japan case). In fact, some CO_2 hotspots could also be seen over major cities of China in WRF–CO_2 simulations, but not many in the ACTM because of smearing out of the anthropogenic emissions in coarse horizontal resolutions in ACTM.

Generally, in the growing (monsoon) season, atmospheric CO_2-uptake during photosynthesis is higher than CO_2-release during respiration. However, in decaying (autumn) season, CO_2-release by plants during respiration is higher than that CO_2-uptake driven by photosynthesis. The land biosphere acts as a source in winter as well as in spring and as a sink in summer over the eastern China (figure 2e–g). However, over South Asia, it generally acts as source in spring and as sink in autumn (figure 2f and h). The monsoonal circulation may lead to cloudy conditions over South Asian region which reduce incoming short wave and outgoing long wave radiation and likely to

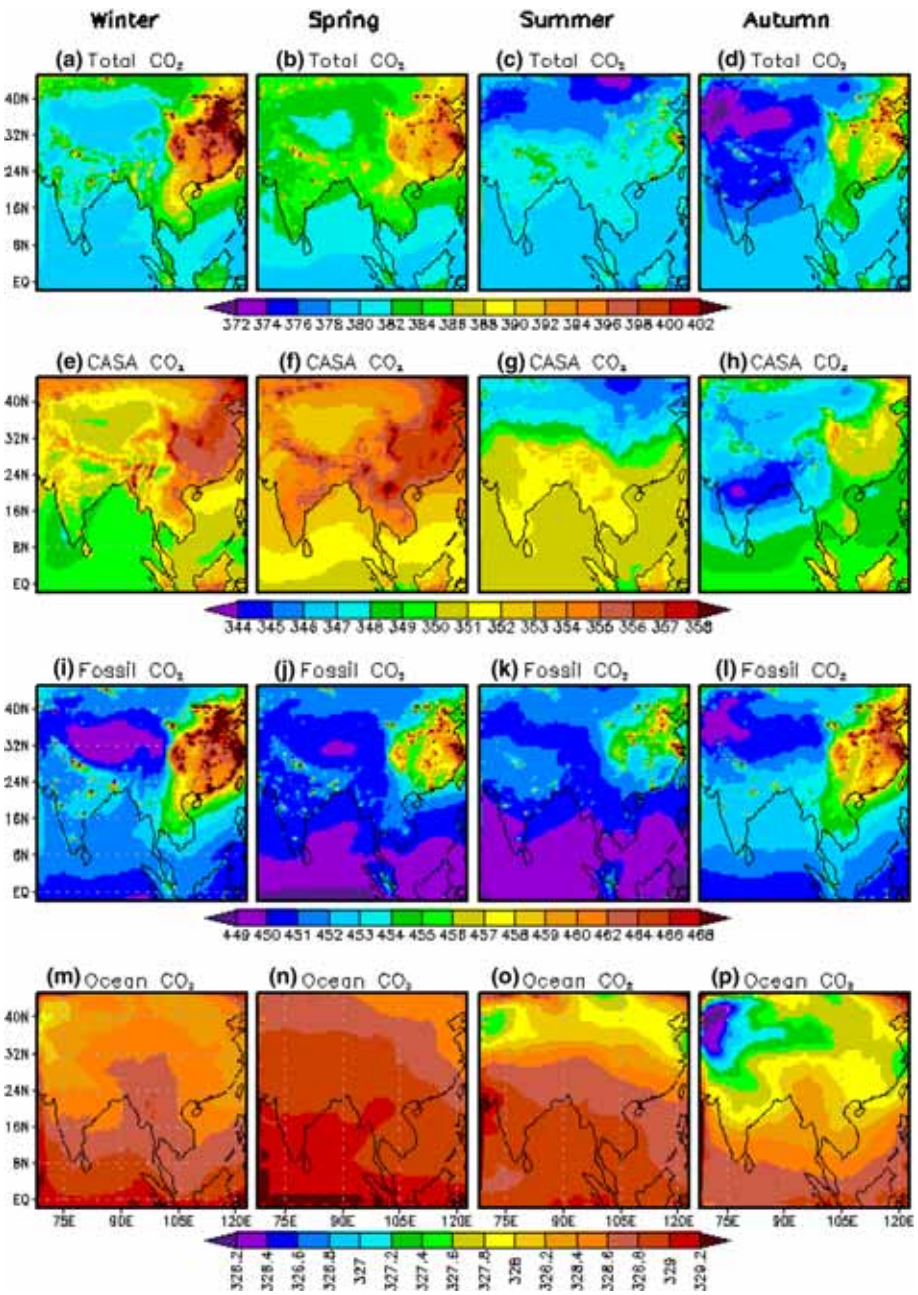

Figure 2. Spatial distribution of total CO_2 mixing ratio (ppm) simulated by the WRF–CO_2 model (top row), and its land biosphere, fossil fuel and ocean flux components (lower 3 panels, respectively) for winter (December–February), spring (March–May), summer (June–August) and autumn (September–November).

decrease the photosynthesis rate in summer monsoon. Subsequently, clear sky in autumn enhances vegetative growth and increases photosynthesis rate leading to decrease in CO_2 (Lin *et al.* 2015). Variation of ocean CO_2 mixing ratio is found to be very small with changing season (about 2.8 ppm) over the domain (figure 2m–p). Therefore, the contribution of ocean CO_2 is smaller to the total CO_2 mixing ratio. In general, ocean CO_2 is highest in spring and lowest in autumn over the domain.

3.2 *Mean seasonal cycle at different sites*

Figure 3 shows the mean seasonal cycle of CO_2 for observations and model simulations at nine sites. Simulation results from the WRF–CO_2 and the ACTM are extracted for the location of these sites (table 1) and compared with observed de-trended monthly mean seasonal cycle of CO_2, at respective sites for three years (2010–2012) period. Hourly (WRF–CO_2) and three hourly (ACTM) data are used to obtain monthly average in case of five sites

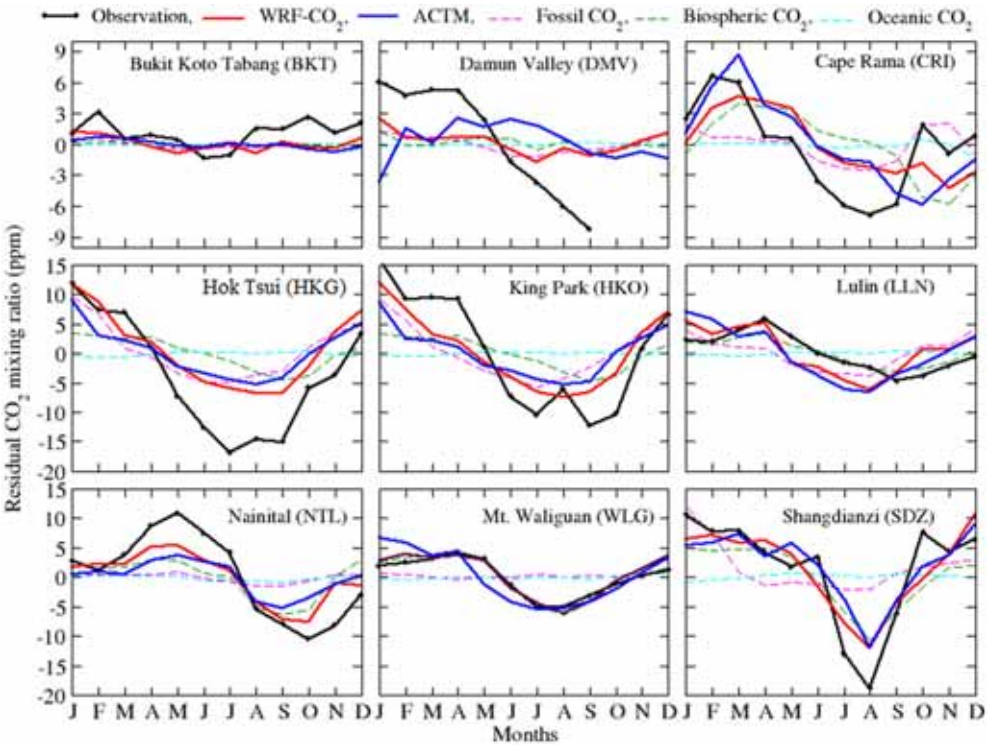

Figure 3. Monthly mean variations of observed and model (WRF–CO_2 and ACTM) CO_2 from three years average de-trend data at nine observation sites. Individual components of CO_2 (ocean, biosphere and fossil) simulated from the WRF–CO_2 model are also shown. Panels are arranged from low (top-left) to high (bottom-right) latitude stations.

(Bukit Koto Tabang (BKT), Damun Valley (DMV), Mt. Waliguan (WLG), Hok Tsui (HKG) and King Park (HKO)), while model data are sampled at the nearest time and date of actual air sample collection at the remaining four sites (Shangdianzi (SDZ), Lulin (LLN), Nainital (NTL) and Cape Rama (CRI)) for obtaining monthly average values.

3.2.1 *Timing of seasonal maximum and minimum*

Most of the observation sites exhibit maximum uptake of CO_2 during late summer and early autumn period and higher values in winter or spring (table 3). Maximum uptake occurs very late (October) for the Himalayan site (NTL) and earliest (June) at the tropical station BKT. The difference in timing of maximum and minimum of CO_2 seasonal cycle in different stations, implies that the stations are influenced by diverse flow of air masses. For example, at NTL, air mass is transported from Middle East and western Asia as well as from Indian subcontinent through monsoon circulation during boreal summer (Kumar *et al.* 2012). Therefore, average seasonal minimum mixing ratio is observed during early October and maximum in the mid-May at this site. However, WLG received strong CO_2 uptake signals from the Siberia region during Jul–Aug–Sep, along with middle eastern and western Asian air masses. Furthermore, this site is influenced by the boundary layer exchanged air mass (Lin *et al.* 2015). The months of CO_2 maximum and minimum produce by the WRF–CO_2 is same as seen in the observations at NTL and WLG, but ACTM shows some differences (table 3). The time of the maximum are found to be better for two stations (BKT and LLN) when actual level of model (WRF–CO_2) for these two sites are considered. This indicates better representation of meteorology and transport by the WRF–CO_2 than the global model ACTM in this region.

At Cape Rama (CRI), mean seasonal cycle is found to be maximum in late February that is almost at end of the north-east monsoon and minimum in late August during the south-west monsoon. This implies that though this site is a tropical coastal station, it is largely influenced by monsoon-driven oceanic air transport to the site and terrestrial ecosystem activity (Bhattacharya *et al.* 2009). In winter, the station received anthropogenic rich CO_2 air mass by long range transport from south-east Asia and north-eastern

Table 3. *Three years average monthly mean CO_2 seasonal amplitudes (in ppm) and month of maximum and minimum in observation and model (WRF–CO_2 and ACTM) simulated CO_2 at BKT, CRI, HKG, HKO, LLN, NTL, WLG and SDZ. Amplitude could not be calculated for DMV due to limited data at this site.*

	Observations			WRF–CO_2			ACTM		
Sites	Amplitude	Month of max	Month of min.	Amplitude	Month of max	Month of min.	Amplitude	Month of max	Month of min.
BKT	4.5	Feb	Jun	2.1	Jan	May	1.6	Feb	Nov
CRI	13.5	Feb	Aug	9.0	Mar	Nov	14.6	Mar	Oct
HKG	28.7	Jan	Jul	18.5	Jan	Sep	14.3	Jan	Aug
HKO	28.2	Jan	Sep	19.4	Jan	Aug	13.8	Jan	Aug
LLN	10.6	Apr	Sep	11.8	Jan	Aug	13.6	Jan	Aug
NTL	21.5	May	Oct	12.9	May	Oct	9.0	May	Sep
WLG	9.3	Apr	Aug	9.9	Apr	Aug	6.8	Jan	Jul
SDZ	29.5	Jan	Aug	22.8	Dec	Aug	20.8	Dec	Aug

Indian subcontinent. Moreover, northern India terrestrial biospheric activity is dominated during winter by the heterotrophic respiration. However, during summer monsoon season, air mass comes from the Arabian Sea and the Indian Ocean and lead to rainfall. Subsequently, vegetative growth takes place and maximum photosynthetic uptake during this season is observed. Such meso-scale phenomena cannot be represented by global models. Tiwari *et al.* (2011) showed that global models' results could not capture the months of seasonal maximum/minimum for CRI. It was also shown that observed minimum in October is due to presence of strong south-westerly wind leading to upwelling at Arabian Sea and a source of Ocean CO_2 (Bhattacharya *et al.* 2009). Some differences in the CO_2 seasonal cycle by the WRF–CO_2 at CRI is likely due to the biospheric flux uncertainty in CASA fluxes. The CASA flux are coarse resolution and having annually balanced net flux. An inverse modelling result suggested earlier peak in land biosphere uptake compared to the CASA model simulation (Patra *et al.* 2011).

3.2.2 *Seasonal amplitude*

It could be seen that seasonal variations are greater at relatively higher latitudes (above 22°N, except at both mountain sites in China, i.e., at WLG and LLN) and it is least at tropical sites (e.g., BKT and DMV) (figure 3 and table 3). Observations exhibit the largest seasonal amplitude in China, at SDZ (29.5 ppm), HKG (28.7 ppm) and HKO (28.2 ppm) followed by NTL (21.5 ppm) (table 3). Seasonal amplitudes are about 14 ppm or lesser at rest of the sites. It can be noted that out of two stations in India, NTL (29.36°N) shows greater seasonal amplitude than at CRI (14 ppm), which is at relatively lower latitude (15.08°N). The strong seasonality in solar insolation and temperature in higher latitudes leads to stronger seasonal variations in photosynthesis (and respiration) by plant in the extra-tropical and midlatitude regions. The seasonality of carbon assimilation is smaller at the sites in lower latitude (CRI, BKT and DMV). The two tropical rainforest stations BKT and DMV show peak-to-trough seasonal amplitude of only $\sim$5 ppm indicating no large contrast in CO_2 uptake or release due to weaker seasonality in the regional climate.

We noted that observed mean CO_2 value is 400.4 ppm at HKO (22.3°N), while it is 393 ppm at HKG (22.2°N) (table 4). Both these sites are separated by only $\sim$15 km of areal distance. The observed mean CO_2 at HKO is greater by about 7 ppm, but the CO_2 seasonal amplitudes is similar at both the sites. HKO is an urban site situated within a highly populated city of Hong Kong (under the influence of fossil fuel emissions), whereas, HKG is a remote coastal site where carbon assimilation could be higher than at an urban site. Thereby lower CO_2 mixing ratio is observed at HKG compared to that of HKO.

The observed seasonal amplitudes are compared with the amplitude obtained by WRF–CO_2 and the ACTM (table 3). Model simulated CO_2 amplitudes are generally lower than the observations. Similar feature of lower amplitude by model simulations is observed for an urban site (Ahmedabad) (Chandra *et al.* 2016). It is also observed that the WRF–CO_2 produced better seasonal amplitude for stations with greater seasonal variations (e.g., SDZ, HKG, HKO and NTL). Difference between the model amplitudes and observations for SDZ, HKG, HKO

Table 4. *Statistical analyses (correlation coefficient (CC) and normalised standard deviation (NSD)) among observed CO_2, the WRF–CO_2 and the ACTM simulated CO_2 at nine observation sites. Normalised standard deviation is calculated with the ratio of model standard deviation by observed standard deviation. In ideal case, it would be 1, in case of overestimation and underestimation NSD would be >1 and <1, respectively. Three years average observed CO_2 mixing ratio (in ppm) are also given in the right-most column.*

	Correlation coefficient (CC)		Normalised standard deviation (NSD)		Observed
Stations	WRF–CO_2	ACTM	WRF–CO_2	ACTM	CO_2 (ppm)
BKT	0.13	0.13	0.44	0.27	398.8
DMV	0.81	−0.07	0.23	0.36	391.4
CRI	0.58	0.53	0.67	0.89	395.8
HKG	0.72	0.87	0.56	0.45	393.0
HKO	0.83	0.77	0.66	0.44	400.4
LLN	0.32	0.32	1.12	1.12	389.5
NTL	0.83	0.83	0.63	0.38	389.3
WLG	0.82	0.81	1.37	1.46	391.9
SDZ	0.81	0.77	0.71	0.70	398.9

and NTL are about 23%, 36%, 31% and 40% for the WRF–CO_2 and 30%, 50%, 51% and 58% for the ACTM, respectively.

Statistical analyses of correlation coefficient (CC) and normalised standard deviation (NSD) between observed and model simulations using monthly mean de-trend three years data (2010–2012) are shown in table 4. Correlation and NSD are more-or-less better for the WRF–CO_2 than the ACTM. Correlation coefficient is very good for the WRF–CO_2 (0.81) compared to ACTM (−0.07) at DMV. Root mean square difference (RMSD) between de-trend observation and model CO_2 data does not show any particular pattern. Maximum and minimum RMSD occurs in different months at all sites. For example, maximum RMSD occurs in November and minimum in September at NTL. However, maximum RMSD is observed in March and minimum in May at HKG. For the ACTM, RMSD is higher than the WRF–CO_2. However, patterns in RMSD are quite similar for both models in many cases (e.g., NTL, HKG, HKO and LLN).

3.2.3 *Positive and negative deviations of CO_2*

Positive and negative deviations (i.e., maximum and minimum difference of monthly average from annual average CO_2 value) in CO_2 mixing ratio are also shown in table 5. Interestingly, LLN shows similar positive and negative deviations, indicating a very symmetric seasonal cycle at this site. Positive and negative deviations differ by ≤0.6 ppm at NTL, HKG and HKO, while this difference is ≤1.4 ppm at BKT and WLG. Largest difference of 9.4 ppm (9.2 *vs.* −18.6 ppm) is seen at SDZ, suggesting dominant sink at this site that could be largely due to vegetative growth in warmer climate in the high latitude Northern Hemisphere. Both positive and negative deviations are better estimated by WRF–CO_2 than ACTM (except at LLN and WLG) when compared with observed values. The positive and negative deviation estimates by the model simulations and its differences with the observations, could be an important constraint for better understanding and improving surface fluxes, model resolution and meteorology, etc., in the CO_2 model simulations.

3.2.4 *Contribution of different components of CO_2*

Figure 3 also shows the de-trend variations in three components of CO_2 (biospheric, fossil and ocean) from the WRF–CO_2 model output. Ocean CO_2 is found to have negligible (<10%) contribution at all observation sites. It is observed that the biospheric flux has dominant contribution (>80%) at observation sites in India (NTL and CRI) and China (SDZ, WLG and LLN). Fossil contribution is found to be very low for BKT and DMV due to greater exposure to the pristine oceanic air. One Indian site (CRI) and two sites in China (LLN and SDZ) show moderate contribution of fossil CO_2. High altitude sites in India (NTL) and China (WLG) do not show significant contribution of fossil CO_2 (<2.4 ppm amplitude). LLN has proximity to Beijing and hence contribution of fossil CO_2 is seen

Table 5. *Year-to-year variations in seasonal amplitude of observed and models (WRF–CO_2 and ACTM) CO_2 mixing ratios (in ppm), obtained from smooth de-trend daily average data, at eight stations. Average positive deviation and negative deviation (i.e., maximum and minimum difference of monthly average from annual average CO_2 value) of amplitude is also shown. Amplitude could not be calculated for DMV due to limited data at this site.*

CO_2 (ppm)	Observed	WRF–CO_2	ACTM	Observed	WRF–CO_2	ACTM
	Hok Tsui (HKG)			King Park (HKO)		
Year-to-year amplitude variation	0.7–2.6	0.3–1.8	0.2–0.9	0.7–4.0	0.5–1.9	0.2–0.9
Positive deviation	14.0	9.2	6.4	12.4	9.3	6.4
Negative deviation	−13.6	−7.7	−5.8	−11.8	−7.7	−5.8
	Lulin (LLN)			Waliguan (WLG)		
Year-to-year amplitude variation	0.0–0.4	2.0–6.4	0.3–0.8	0.1–0.3	1.2–4.7	0.1–0.5
Positive deviation	5.1	5.1	6.5	4.4	3.5	5.9
Negative deviation	−5.1	−6.5	−6.6	−5.8	−6.5	−5.6
	Shangdianzi (SDZ)			Nainital (NTL)		
Year-to-year amplitude variation	1.2–5.1	0.1–0.5	0.5–1.5	1.7–4.9	0.7–4.1	0.0–0.2
Positive deviation	9.2	7.1	6.5	10.6	5.6	3.7
Negative deviation	−18.6	−10.9	−13.7	−10.1	−8.7	−4.9
	Bukit Koto Tabang (BKT)			Cape Rama (CRI)		
Year-to-year amplitude variation	0.7–1.6	0.1–0.5	0.2–0.4	0.5–3.3	0.8–1.9	0.5–1.5
Positive deviation	1.7	1.7	0.9	7.3	4.8	6.3
Negative deviation	−2.5	−0.7	−0.9	−7.8	−3.4	−5.8

(∼8 ppm amplitude against 10.6 ppm observed) despite of being high altitude site. Both fossil and biospheric CO_2 have major contributions in CO_2 seasonal cycle amplitude for HKO and HKG, though amplitude of fossil fuel CO_2 (∼15 ppm) is higher than the biospheric CO_2 (∼8 ppm).

Study also shows biospheric CO_2 are in phase with observed atmospheric CO_2, compared to other two fluxes, for the stations NTL, WLG, LLN and SDZ. However, more detailed study about which surface fluxes have major influence into the seasonal variation of CO_2 mixing ratio can be assessed through a footprint analysis (Mukherjee *et al.* 2015). While comparing the WRF–CO_2 spatio-temporal distributions with the ACTM simulations, it is found that the patterns of seasonal changes of different components of CO_2 are quite similar over the domain for both the models but in most of the cases, the WRF–CO_2 simulated CO_2 amplitudes are higher than the ACTM.

3.3 *Inter-annual and seasonal variabilities*

Figure 4 shows inter-annual variations in CO_2 seasonal cycle (observed and model) from three years' time series (2010–2012), obtained after removing secular CO_2 increase rate. Smooth de-trend inter-annual variation of seasonal cycle of observed and simulated CO_2 (WRF–CO_2 and ACTM) are presented in figure 5. Range of observed and modelled (WRF–CO_2 and ACTM) year-to-year variations of seasonal amplitude in CO_2 are also presented in table 5.

Year-to-year variations of CO_2 seasonal amplitude at sites of similar latitudinal belt are differing from one another due to different climatic/meteorological condition, changing geographical location and human activity and hence the amount of CO_2 uptake and release. For example, remote mountain site WLG shows relatively lower seasonal amplitude (9.3 ppm) with lower year-to-year amplitude variation (0.1–0.3 ppm), while continental sites SDZ and NTL show every high seasonal (29.5 and 21.5 ppm) amplitude and inter-annual variations in the amplitude (1.2–5.1 and 1.7–4.9) (figure 4 and table 5). WLG is situated in a temperate climate of the Tibetan Plateau with arid and semi-arid grassland, where the land use remains unchanged for a long time. As a result, within about 100 km radius there is no major biospheric and fossil CO_2 source/sink and hence the lower seasonal cycle amplitude as well as less variations in the amplitude. Observation data at SDZ was taken 150 km northeast of Beijing and NTL is located 225 km northeast of Delhi. Therefore, these two stations have high possibility of large scale transport of anthropogenic CO_2 tracer with dominant winds from the megacities in addition to the large regional biospheres. In addition, observed CO_2 mixing ratio maxima is found to be varying with year at SDZ, implying strong local source of CO_2 as well (figure 5).

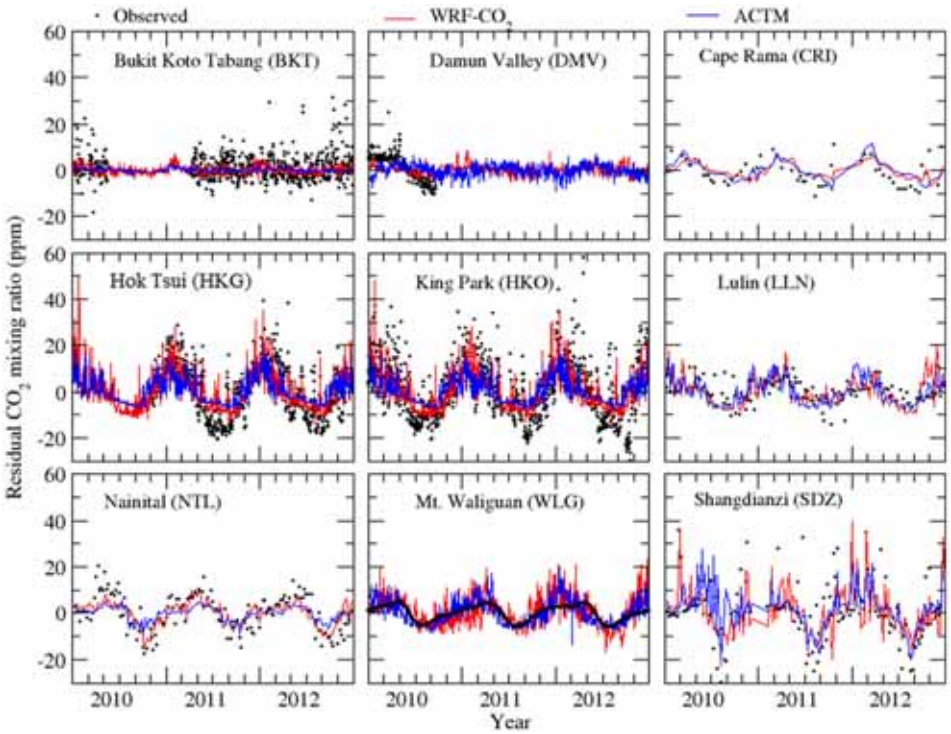

Figure 4. De-trended inter-annual variation of seasonal cycle of CO_2 obtained after removing the secular CO_2 increase rate by digital filtering technique (Nakazawa *et al.* 1997) from the model and observed data (2010–2012) at nine sites.

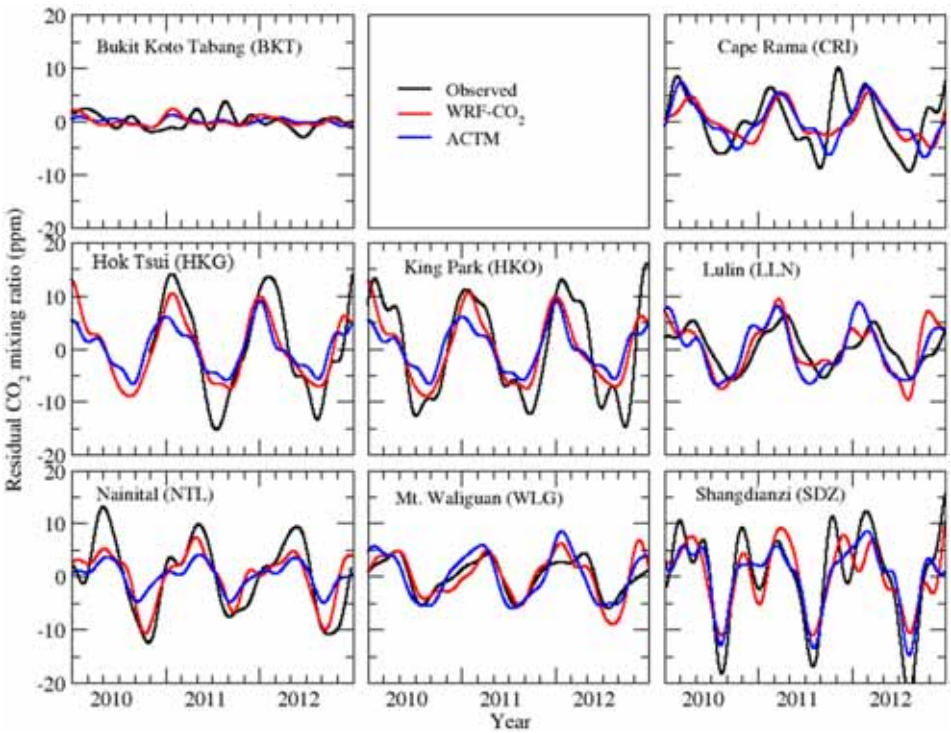

Figure 5. Smooth detrended inter-annual variation of seasonal cycle of CO_2 mixing ratio of observed and model (WRF–CO_2 and ACTM) simulations in different sites for 2010–2012, obtained from fitted curve of digital filtering.

At WLG, the ACTM simulated year-to-year difference in amplitude is reasonable (≤0.5 ppm), but it is quite large (1.2–4.7 ppm) for the WRF–CO_2. But in case of SDZ, year-to-year difference in amplitude is not well represented by both the models. The year-to-year difference is

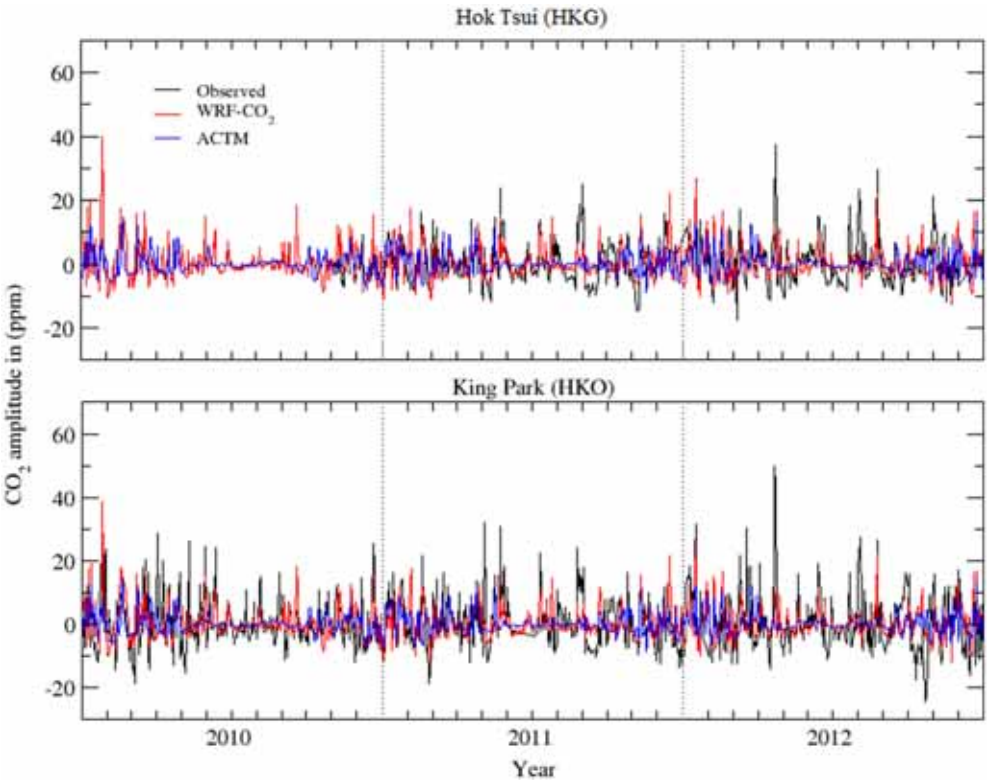

Figure 6. Observed and models (WRF–CO_2 and ACTM) synoptic scale variation of CO_2 at Hok Tsui (HKG) and King Park (HKO), derived from subtracting the raw data from the fitted data. Observational data is not available during early 2010 at HKG.

reasonable by WRF–CO_2 (about ∼4 ppm) than by ACTM (about 0.2 ppm) at NTL. The observed year-to-year variations of seasonal amplitude at another mountain site in China is also found to be very small (≤0.4 ppm). This smaller variability could be due to lesser inter-annual variability in ecosystem in the region. The ACTM simulated year-to-year difference in amplitude is reasonable (≤0.8 ppm), but quite large (about 6.4 ppm) for the WRF–CO_2.

The observed seasonal amplitudes of CO_2 are approximately similar for HKG and HKO (shown in table 3 with year-to-year difference in amplitudes is in the range of 0.7–2.6 and 0.7–4.0 ppm, respectively. The WRF–CO_2 and the ACTM simulated amplitude show year-to-year difference of about 2.0 and 0.9 ppm, respectively. Year-to-year variation of CO_2 is moderate (about 1.6 and 3.3 ppm) at the tropical sites (BKT and CRI). However, both the models show quite low variations (≤0.5 and ≤1.9) than in the observations.

3.4 *Synoptic scale variation of CO_2*

The synoptic variations are studied by removing trend and seasonality from the daily average CO_2 time series using the digital filter. The daily averaging removes small scale effects such as eddies; those are not resolved by the models and signal from diurnal variation of biospheric flux in terms of photosynthesis and respiration. Figure 6 shows synoptic scale variations at two sites (HKG and HKO) where greater variability in CO_2 with a deeper seasonal cycle is noted and more importantly data are available at daily or shorter time intervals.

Synoptic scale variation of CO_2 mixing ratio is higher in the downwind regions. Therefore, synoptic scale variations are observed to be greater generally during late winter/early spring and late autumn at HKG and HKO due to transport of pollutant from East Asia by the Asian winter monsoon. The variations are more-or-less similar at these two sites in Hong Kong with quite low variations during summer. This could be due to spatial closeness of both sites. Winter time high variability is due to the strong fossil emission signal from highly populated city centre of Hong Kong. The WRF–CO_2 is found to capture peaks and troughs better than the ACTM for these two sites.

The synoptic scale variations are further studied during afternoon (1300–1600 hr) and night-time

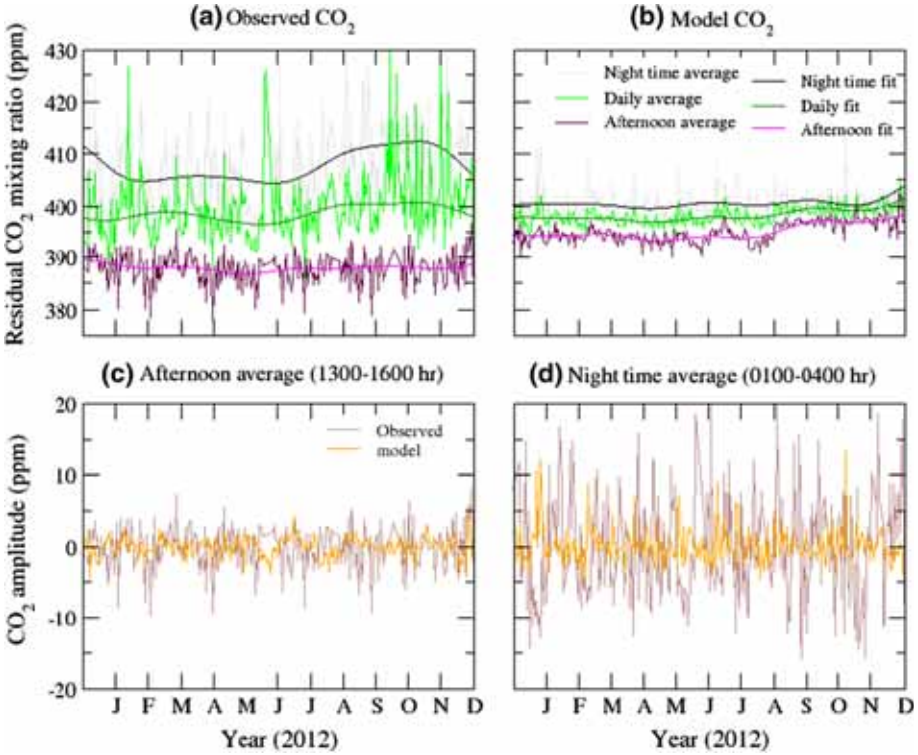

Figure 7. **(a)** Observed and **(b)** the WRF–CO_2 model simulated seasonal cycle and fitted curve of CO_2 using daily average, afternoon average and night-time average data at Bukit Koto Tabang (BKT) for the year 2012. **(c)** Observed and model synoptic scale variation of CO_2 using afternoon average data and **(d)** night-time average data.

(0100–0400 hr) to see the model performance in comparison to the observation (figure 7). The high frequency (hourly) continuous data for a complete year are available only at BKT. It is found that the WRF–CO_2 model is able to simulate afternoon variations (figure 7c); however, it is not able to show large variations in night-time (figure 7d) as observed, though the night-time value is higher than daytime.

Model simulated night-time values are also lower than the observed values. Lower CO_2 mixing ratio and lower amplitude at night-time is likely due to the overestimation of the planetary boundary layer height by the model during the night. It is noted by other model studies that night-time shallow boundary layer contributes for greater mismatch between model results and observations (Thoning *et al.* 1989; Gerbig *et al.* 2008; Kretschmer *et al.* 2014). It was shown that the boundary layer mixing height has greater biases during night-time (40–60%) when compared with daytime (10–20%) that will lead to uncertainty of several ppm for CO_2 (Gerbig *et al.* 2008). The afternoon and daily average variations are fairly similar and likely to be the better representative of the synoptic scale variation of CO_2 (Patra *et al.* 2008). Our results are also consistent with previous studies suggesting that the stations situated in the free troposphere likely to show closer model–observation agreement at night than during the day (Patra *et al.* 2008; Chevallier *et al.* 2010). This suggests a need for improvement in mixing layer height parameterization scheme for better simulating both the day- and night-time concentration of CO_2 (Ballav *et al.* 2016). The present study also calls for more observations at high frequency (sub-daily time intervals) at the different locations of the domain to better understand the limitation and advantages of WRF–CO_2 model simulation.

4. Summary and conclusions

An online tracer transport model WRF–CO_2 is set up over a greater Asia region for CO_2 simulation during the years 2010–2012 to investigate the variations in atmospheric CO_2 mixing ratio. Three different components of CO_2 fluxes, namely ocean exchange, biosphere fluxes and fossil-fuel consumption, are treated in the model as non-reactive tracers whose mixing ratio are calculated from atmospheric transport with standard set of parameterization. The WRF–CO_2 model results are compared with observations at nine observations sites from different geographical locations in

South/Southeast/East Asia and global Atmospheric Chemistry Transport Model's (ACTM) data.

It is shown that the observed CO_2 seasonal variations are different over the study region and seasonal amplitudes are observed to be >10 ppm at most of the sites. The majority of the sites exhibit maximum uptake of CO_2 during late summer or early autumn period and higher CO_2 values in winter or spring with some differences between South and East Asia. It is also seen that seasonal variations are greater at relatively higher latitudes and it is least at southern most sites. Eastern China shows very high CO_2 values in winter that could be due to greater energy consumption. While CO_2 values over South Asia is lower than those in eastern China and it occurs in spring. On the other hand, observations in East Asia show that CO_2 seasonal variation is not much influenced by local sources, rather by the sources and sinks over a very large region (Nomura *et al.* 2017). In general, the WRF–CO_2 model predicted seasonal amplitudes are somewhat lower than those observed, but better than those from ACTM simulation. More specifically, it is noted that the WRF–CO_2 produced better results than ACTM, particularly for stations with greater seasonal variations (e.g., Shangdianzi, Hok Tsui and King Park). Further, the WRF–CO_2 produces better results than the ACTM over regions of complex topography (e.g., Nainital). Correlation coefficients between observed and the WRF–CO_2 are generally better or equal than those between observed and the ACTM.

Impact assessment on mean seasonal variation of CO_2 by different prescribe fluxes show that the contribution of biospheric and fossil CO_2 are somewhat similar at high latitude urban stations. However, dominant contribution of biospheric flux is noted at WLG, NTL, SDZ, and LLN (>80%). Oceanic CO_2 showed least contribution at all sites (<10%). Model is able to produce seasonal amplitude, timing of maximum/minimum and thereby able to identify whether the station is behaving as source or sink. Synoptic scale variations are better predicted by WRF–CO_2 than the ACTM. Daytime CO_2 variations are seen to be much smaller than night-time CO_2 and the WRF–CO_2 also shows better agreement in daytime data.

The results demonstrated that the WRF–CO_2 is able to resolve fine scale features of CO_2 variation and is facilitating interpretation of seasonal, interannual and synoptic scale variation of CO_2 observations better than the global model ACTM. This study also highlights the requirement of input flux with resolution close to the model grid, in addition with high temporal and vertical variation, for proper representation of flux, particularly biospheric flux. This is more important for regions with highly varying topography and ecosystem like in the Himalayas and coastal sites, for realistic representation of CO_2 over South Asian region. It is well established that changing weather, climate and human activity could influence terrestrial biospheric exchange and hence CO_2 amount. These results from the WRF–CO_2 simulation could be useful for inverse calculation of CO_2 source and sink in order to reduce the uncertainty in flux estimation.

Acknowledgements

SB acknowledges support by the Grants-in-Aid for creative scientific research (Grant no. PDF/2016/003032) of SERB-DST under NPDF scheme, Gov. of India. Support from Director ARIES and ISRO-ATCTM project is highly acknowledged. We are thankful to S Nomura, Y Terao, N Ojha and Kalpana for their help in observations at Nainital. We are grateful to Prof. Shyam Lal, PRL for his fruitful comments on the manuscript. The CO_2 measurements (eight sites) used in this study are obtained from WDCGG (ds.data.jma.go.jp/gmd/wdcgg/). We wish to thank Hong Kong Observatory (HKO), Malaysian Meteorological Department (MMD), Indonesia Agency for Meteorology, Climate and Geophysics (BMKG), Meteorological Observation Centre of China Meteorological Administration (CMA), Lulin Atmospheric Background Station (LABS), Global Monitoring Division ESRL NOAA and the Commonwealth Scientific and Industrial Research Organisation (CSIRO) for making observations at their respective sites and acknowledge them for providing data through WDCGG. We are also thankful to both the reviewers for their constructive comments.

References

Ballav S, Patra P K, Takigawa M, Ghosh S, De U K, Murayama S, Mukai H and Hashimoto S 2012 Simulation of CO_2 mixing ratio over east Asia region using the Regional Transport Model WRF–CO_2; *J. Meteorol. Soc. Japan* **90(6)** 959–976.

Ballav S, Patra P K, Sawa Y, Matsueda H, Adachi A, Onogi S, Takigawa M and De U K 2016 Simulation of CO_2 mixing ratios at Tsukuba tall tower using WRF–CO_2 tracer transport model; *J. Earth Syst. Sci.* **125** 47–64.

Barnston A G, Li S, Mason S J, Dewitt D G, Goddard L and Gong X 2010 Verification of the first 11 years of IRI's seasonal climate forecasts; *J. Appl. Meteorol. Clim.* **49** 493–520.

Bhattacharya S K, Borole D V, Francey R J, Allison C E, Steele L P, Krummel P, Langenfelds R, Masarie K A, Tiwari Y K and Patra P K 2009 Trace gases and CO_2 isotope records from Cabo de Rama, India; *Curr. Sci.* **97(9)** 1336–1344.

Chevallier F, Breon F M and Rayner P J 2010 CO_2 surface fluxes at grid point scale estimated from a global 21-year reanalysis of atmospheric measurements; *J. Geophys. Res.* **115** D2137.

Chandra N, Lal S, Venkataramani S, Patra P K and Sheel V 2016 Temporal variations of atmospheric CO_2 and CO at Ahmedabad in western India; *Atmos. Chem. Phys.* **16** 6153–6173.

Chandra N, Hayashida S, Saeki T and Patra P K 2017 What controls the seasonal cycle of columnar methane observed by GOSAT over different regions in India?; *Atmos. Chem. Phys.* **17** 12,633–12,643.

Dlugokencky E J, Lang P M, Mund J W, Crotwell A M, Crotwell M J and Thoning K W 2017 Atmospheric carbon dioxide dry air mole fractions from the NOAA ESRL carbon cycle cooperative global air sampling network, 1968–2016, Version: 2017-07–28, Path: ftp://aftp.cmdl.noaa.gov/data/trace_gases/co2/flask/surface/.

EDGAR4.2: Emission Database for Global Atmospheric Research (EDGAR), release version 4.2 2011 European Commission, Joint Research Centre (JRC)/Netherlands Environmental Assessment Agency (PBL), http://edgar.jrc.ec.europa.eu.

Gerbig C, Körner S and Lin J C 2008 Vertical mixing in atmospheric tracer transport models: Error characterization and propagation; *Atmos. Chem. Phys.* **8** 591–602.

Grell G A, Peckham S E, Schmitz R, McKeen S A, Frost G, Skamarock W C and Eder B 2005 Fully coupled 'online' chemistry within the WRF model; *Atmos. Environ.* **39** 6957–6975.

IPCC: Climate Change 2014 Impacts, adaptation, and vulnerability. Part B: Regional aspects; Contribution of Working Group II to the Fifth Assessment Report of the Intergovermental panel on Climate Change (eds) Barros V R and Field C B *et al.*, Cambridge University Press, Cambridge, United Kingdom and New York, NY, USA.

Joos F and Spahni R 2008 Rate of change in natural and anthropogenic radiative forcing over the past 20,000 years; *Proc. Natl. Acad. Sci. USA* **105** 1425–1430.

King A W, Andres R J, Davis K J, Hafer M, Hayes D J, Huntzinger D N, de Jong B, Kurz W A, McGuire A D, Vargas R, Wei Y, West T O and Woodall C W 2015 North America's net terrestrial CO_2 exchange with the atmosphere 1990–2009; *Biogeosci.* **12** 399–414.

Kou X, Zhang M, Peng Z and Wang Y 2015 Assessment of the biospheric contribution to Surface Atmospheric CO_2 mixing ratios over East Asia with a regional chemical transport model; *Adv. Atmos. Sci.* **32** 287–300.

Kretschmer R, Gerbig C, Karstens U, Biavati G, Vermeulen A, Vogel F, Hammer S and Totsche K U 2014 Impact of optimized mixing heights on simulated regional atmospheric transport of CO_2; *Atmos. Chem. Phys.* **14** 7149–7172.

Krishnamurti T N, Bedi H S and Hardiker V M 1998 *An introduction to global spectral modeling*; Oxford University Press, Oxford, pp. 11–13.

Kumar R, Naja M, Pfister G G, Barth M C and Brasseur G P 2012 Simulations over South Asia using the Weather Research and Forecasting model with Chemistry (WRF-Chem): Set-up and meteorological evaluation; *Geosci. Model Dev.* **5** 321–343.

Le Quéré C, Andrew R M, Friedlingstein P, Sitch S, Hauck J, Pongratz J, Pickers P A, Korsbakken J I, Peters G P, Canadell J G, Arneth A, Arora V K, Barbero L, Bastos A, Bopp L, Chevallier F, Chini L P, Ciais P, Doney S C, Gkritzalis T, Goll D S, Harris I, Haverd V, Hoffman F M, Hoppema M, Houghton R A, Hurtt G, Ilyina T, Jain A K, Johannessen T, Jones C D, Kato E, Keeling R F, Goldewijk K K, Landschützer P, Lefèvre N, Lienert S, Liu Z, Lombardozzi D, Metzl N, Munro D R, Nabel J E M S, Nakaoka S-i, Neill C, Olsen A, Ono T, Patra P, Peregon A, Peters W, Peylin P, Pfeil B, Pierrot D, Poulter B, Rehder G, Resplandy L, Robertson E, Rocher M, Rödenbeck C, Schuster U, Schwinger J, Séférian R, Skjelvan I, Steinhoff T, Sutton A, Tans P P, Tian H, Tilbrook B, Tubiello F N, van der Laan-Luijkx I T, van der Werf G R, Viovy N, Walker A P, Wiltshire A J, Wright R, Zaehle S and Zheng B 2018 Global Carbon Budget 2018; *Earth Syst. Sci. Data* **10** 2141–2194.

Lin X, Indira N K, Ramonet M, Delmotte M, Ciais P, Bhatt B C, Reddy M V, Angechuk D, Balakrishnan S, Jorphail S, Dorjai T, Mahey T T, Patnaik S, Begum M, Brenninkmeijer C, Durairaj S, Kirubagaran R, Schmidt M, Swathi P S, Vinithkumar N V, Yver Kwok C and Gaur V K 2015 Long-lived atmospheric trace gases measurements in flask samples from three stations in India; *Atmos. Chem. Phys.* **15** 9819–9849.

Luyssaert S, Abril G, Abdres R, Bastviken D, Bellassen V, Bergamaschi P, Bousquet P, Chevallier F, Ciais P, Carazza M and Dechow R *et al.* 2012 The European land and inland water CO_2, CO, CH_4 and N_2O balance between 2001 and 2005; *Biogeosci.* **9** 3357–3380.

Mukherjee S, McMillan A M S, Sturman A P, Harvey M and Laubach J 2015 Footprint methods to separate N_2O emission rates from adjacent paddock areas; *Int. J. Biomet.* **59(3)** 325–338.

Naja M, Bhardwaj P, Singh N, Kumar P, Kumar R, Ojha N, Sagar R, Satheesh S K, Krishna Moorthy K and Kotamarthi V R 2016 High-frequency vertical profiling of meteorological parameters using AMF1 facility during RAWEX–GVAX at ARIES, Nainital; *Curr. Sci.* **111(1)** 132–140.

Niwano M, Takigawa M, Takahashi M, Akimoto H, Nakazato M, Nagai T, Sakai T and Mano Y 2007 Evaluation of vertical ozone profiles simulated by WRF/Chem using Lidar-observed data; *SOLA* **3** 133–136, https://doi.org/10.2151/sola.2007-034.

Nomura S, Mukai H, Terao Y, Machida T and Nojiri Y 2017 Six years of atmospheric CO_2 observations at Mt. Fuji

recorded with a battery-powered measurement system; *Atmos. Meas. Tech.* **10** 667–680.

Nakazawa T, Ishizawa M, Higuchi K and Travett N B A 1997 Two curve fitting methods applied to CO_2 flask data; *Environmetrics* **8** 197–218.

Olsen S C and Randerson J T 2004 Differences between surface and column atmospheric CO_2 and implications for carbon cycle research; *J. Geophys. Res.* **109** D02301.

Patra P K, Law R M, Peters W, Rödenbeck C, Takigawa M, Aulagnier C, Baker I, Bergmann D J, Bousquet P, Brandt J, Bruhwiler L, Cameron-Smith P J, Christensen J H, Delage F, Denning A S, Fan S, Geels C, Houweling S, Imasu R, Karstens U, Kawa S R, Kleist J, Krol M C, Lin S-J, Lokupitiya R, Maki T, Maksyutov S, Niwa Y, Onishi R, Parazoo N, Pieterse G, Rivier L, Satoh M, Serrar S, Taguchi S, Vautard R, Vermeulen A T and Zhu Z 2008 TransCom model simulations of hourly atmospheric CO_2: Analysis of synoptic scale variation for the period 2002–2003; *Global Biogeochem. Cycle* **22(4)** GB4013.

Patra P K, Takigawa M, Ishijima K, Choi B-C, Cunnold D, Dlugokencky E J, Fraser P, Gomez-Pelaez A J, Goo T-Y, Kim J-S, Krummel P, Langenfelds R, Meinhardt F, Mukai H, O'Doherty S, Prinn R G, Simmonds P, Steele P, Tohjima Y, Tsuboi K, Uhse K, Weiss R, Worthy D and Nakazawa T 2009 Growth rate, seasonal, synoptic, diurnal variations and budget of methane in lower atmosphere; *J. Meteorol. Soc. Japan* **87** 635–663.

Patra P K, Niwa Y, Schuck T J, Brenninkmeijer C A M, Machida T, Matsueda H and Sawa Y 2011 Carbon balance of South Asia constrained by passenger aircraft CO_2 measurements; *Atmos. Chem. Phys.* **11** 4163–4175.

Patra P K, Canadell J G, Houghton R A, Piao S L, Oh N-H, Ciais P, Manjunath K R, Chhabra A, Wang T, Bhattacharya T, Bousquet P, Hartman J, Ito A, Mayorga E, Niwa Y, Raymond P A, Sarma V V S S and Lasco R 2013 Carbon budget of south Asia; *Biogeosci.* **10** 513–527.

Pillai D, Gerbig C, Marshall J, Ahmadov R, Kretschmer R, Koch T and Karstens U 2009 High resolution modeling of CO_2 over Europe: Implications for representation errors of satellite retrievals; *Atmos. Chem. Phys.* **10(1)** 83–94.

Sarrat C, Noilhan J, Dolman A J, Gerbig C, Ahmadov R, Tolk L F, Meesters A, Hutjes R W A, Ter Maat H W, Perez-Landa G and Donier S 2007 Atmospheric CO_2 modeling at the regional scale: An intercomparison of 5 meso-scale atmospheric models; *Biogeosci.* **4(6)** 1115–1126.

Sitch S *et al.* 2008 Evaluation of the terrestrial carbon cycle, future plant geography and climate-carbon cycle feedbacks using 5 dynamic global vegetation models (DGVMs); *Global Change Biol.*, https://doi.org/10.1111/j.1365-2486.2008.01626.x.

Sundareshwar P V, Murtugudde R, Srinivasan G, Singh S, Ramesh K J, Ramesh R, Verma S B, Agarwal D, Baldocchi D, Baru C K, Baruah K K, Chowdhury G R, Dadhwal V K, Dutt C B S, Fuentes J, Gupta P K, Hargrove W W, Howard M, Jha C S, Lal S, Michener W K, Mitra A P, Morris J T, Myneni R R, Naja M, Nemani R, Purvaja R, Raha S, Santhana Vanan S K, Sharma M, Subramaniam A, Sukumar R, Twilley R R and Zimmerman P R 2007 Environmental monitoring network for India; *Science* **316** 204–205.

Takahashi T, Sutherland S C, Wanninkhof R, Sweeney C, Feely R A, Chipman D W, Hales B, Friederich G, Chavez F, Sabine C, Watson A, Bakker D C E, Schuster U, Metzl N, Yoshikawa-Inoue H, Ishii M, Midorikawa T, Nojiri Y, Körtzinger A, Steinhoff T, Hoppema M, Olafsson J, Arnarson T S, Tilbrook B, Johannessen T, Olsen A, Bellerby R, Wong C S, Delille B, Bates N R and de Baar H J W 2009 Climatological mean and decadal change in surface ocean pCO_2, and net sea–air CO_2 flux over the global oceans; *Deep-Sea Res. II* **56** 554–577.

Takigawa M, Niwano M, Akimoto H and Takahashi M 2007 Development of one way nested global-regional air quality forecasting model; *SOLA* **3** 81–84.

Thoning K W, Pieter P T and Walter D K 1989 Atmospheric carbon dioxide at Mauna Loa Observatory: 2. Analysis of the NOAA GMCC data, 1974–1985; *J. Geophys. Res.* **94(6)** 8549–8565.

Tiwari Y K, Patra P K, Chevallier F, Francey R J, Krummel P B, Allison C E, Revadekar J V, Chakraborty S, Langenfelds R L, Bhattacharya S K, Borole D V, Kumar K R and Steele L P 2011 Carbon dioxide observations at Cape Rama, India for the period 1993–2002: Implications for constraining Indian emissions; *Curr. Sci.* **101(12)** 1562–1568.

Umezawa T, Niwa Y, Sawa Y, Machida T and Matsueda H 2016 Winter crop CO_2 uptake inferred from CONTRAIL measurements over Delhi, India; *Geophys. Res. Lett.* **43(22)** 11,859–11,866.

WDCGG 2016 World Data Center for Greenhouse Gases, World Meteorological Organization (WMO) Global Atmospheric Watch (GAW), Japan Meteorological Agency (JMA), http://ds.data.jma.go.jp/gmd/wdcgg.

Corresponding editor: N V Chalapathi Rao